

Article

# Effect of Zr Target Current on the Mechanical and Tribological Performance of MoS<sub>2</sub>–Zr Composite Lubricating Coatings

Wenlong Song <sup>1,2,\*</sup>, Zixiang Xia <sup>1</sup>, Shoujun Wang <sup>1</sup> and Qingge Zhang <sup>1</sup>

<sup>1</sup> Department of Mechanical Engineering, Jining University, Qufu 273155, China; xiazixiang168@163.com (Z.X.); shoujun0531@163.com (S.W.); zqgsst@126.com (Q.Z.)

<sup>2</sup> Department of Material Science & Engineering, Shandong University, Jinan 250061, China

\* Correspondence: wlsong@jnxu.edu.cn

Received: 18 December 2019; Accepted: 17 January 2020; Published: 18 January 2020



**Abstract:** To improve the tribological properties of pure MoS<sub>2</sub> coating, the MoS<sub>2</sub>–Zr composite lubricating coatings were prepared on the WC/TiC/Co carbide surface utilizing radio frequency magnetron sputtering method combining with multiple arc ion plating technology. The effects of different Zr target currents on the surface morphologies, roughness, Zr content, adhesive force, thickness, microhardness and tribological behaviors of the composite coatings were systematically investigated. Results showed that the properties of MoS<sub>2</sub> coating can be remarkably enhanced through co-deposition of a certain amount of Zr. As the Zr target current increased, the Zr content, surface roughness, thickness, and micro-hardness gradually increased, while the adhesive force of coatings increased first and then decreased. The friction behaviors and wear modes of the composite coatings both varied obviously with the increase of Zr current. The mechanism was mainly attributed to the different components and mechanical properties of the coatings caused by various Zr current.

**Keywords:** MoS<sub>2</sub>–Zr lubricating coatings; Zr target current; mechanical performance; tribological properties

## 1. Introduction

Surface coatings prepared by physical vapor deposition (PVD) can improve physical and mechanical properties, and expand the industry applications of traditional material [1]. According to the material characteristics, the coatings can be classified into two primary types: hard coatings and lubricating coatings.

With higher hardness, excellent wear resistance and high-temperature stability, the hard coatings have been extensively applied to prolong the service lifetime of engineering products. Early hard coatings are mainly composed of binary nitrides, carbides, and oxides such as TiN [2], TiC [3] and Al<sub>2</sub>O<sub>3</sub> [4]. With the rapid development of material science and coating technology, the multi-component composite coatings and multilayer composite coatings, such as TiCN [5], AlCrN [6], TiAlN [7,8], CrSiCN [9], TiAlSiN [10–12] and so on [13], have attracted increasing research, which exhibit much higher surface hardness and more excellent tribological properties.

With the advantages of low friction coefficient and self-lubrication capability, the lubricating coatings have been considered to be a very promising alternative to improve the friction and wear characteristics of substrate, such as tungsten disulfide (WS<sub>2</sub>) [14–16], graphite [17] and Molybdenum disulfide (MoS<sub>2</sub>) [18,19]. As a widely known solid lubricant material, MoS<sub>2</sub> is extensively applied in various fields such as lubricant additives, burnished coatings, and deposited coatings through the PVD method [20–22]. However, the solid or liquid lubricants containing MoS<sub>2</sub> with additives cannot

apply to some practical applications with severe cleanliness or environmental restrictions. Due to the intrinsic properties of poor adhesion to substrate and non-uniformity distribution, burnished coatings cannot supply satisfied lubricating effect and service lifetime. PVD method is then considered to be the most effective technique to fabricate the MoS<sub>2</sub> lubricating coating. The lubricating coating has been widely applied in vacuum and dry environment. In order to enhance the tribological properties of pure MoS<sub>2</sub> coating, an appropriate amount of metal has been added into the sulfide matrix. Because of the addition of metal, the MoS<sub>2</sub>-metal lubricating coatings, such as MoS<sub>2</sub>-Ti [23–25], MoS<sub>2</sub>-Cr [26,27], MoS<sub>2</sub>-W [28], MoS<sub>2</sub>-Zr [29–33], MoS<sub>2</sub>-Ni [34] and MoS<sub>2</sub>-Pb [35], exhibit better properties in surface hardness and wear resistance, and have been successfully used in the machining field, such as drilling and turning.

Based on the theoretical and experimental studies, the MoS<sub>2</sub>-Zr lubricating coatings through adding Zr additives can effectively enhance the tribological properties in sliding wear tests [29,30] and dry cutting tests [31,32]. Meanwhile, the effects of test conditions [29,33], such as applied load and sliding speed, on the tribological behaviors were also studied. The MoS<sub>2</sub>-Zr composite coatings have been mainly applied in the intermittent cutting and continuous low-speed machining due to the sensitivity to high temperature (>550 °C) [31]. However, the optimal deposition conditions of the MoS<sub>2</sub>-Zr lubricating coatings, such as Zr target current, and the influence mechanisms have not been studied. Hence, to further improve the properties of the MoS<sub>2</sub>-Zr lubricating coatings and make the best use of the coatings, the effects of Zr current on the surface morphologies, roughness, Zr content, adhesive force, thickness, microhardness and tribological behaviors of the MoS<sub>2</sub>-Zr coatings were systematically investigated in this work. Results can offer some beneficial information for further industrial application of the lubricating coatings.

## 2. Materials and Methods

### 2.1. Coating Preparation

WC/TiC/Co cemented carbide was utilized as the substrate material. Table 1 shows the main physical and mechanical properties of the WC/TiC/Co substrate. After mirror polishing and ultrasonic cleaning, the carbide samples were placed in the Multiple Use Plating Equipment (AS-585, Dalian Vacuum Technology Co., Ltd., Dalian, China), which combined the radio frequency magnetron sputtering technology (MS) and multiple arc ion plating method (IP). To prepare the MoS<sub>2</sub>-Zr composite lubricating coatings, two pure MoS<sub>2</sub> targets (MS), one Ti target (IP) and one Zr target (IP) were employed. A thin Ti transition layer was deposited first for 5 min to modify the adhesive force between the coatings and carbide substrate. The process parameters of the lubricating coatings are displayed in Table 2.

**Table 1.** Properties of the cemented carbide material.

Composition (wt.%)	Density (g/cm <sup>3</sup> )	Hardness (GPa)	Flexural Strength (MPa)	Young's Modulus (GPa)	Thermal Expansion Coefficient (10 <sup>-6</sup> /K)	Poisson's Ratio
WC + 15%TiC + 6%Co	11.5	15.5	1130.0	510.0	6.51	0.25

**Table 2.** The coating deposition conditions.

Substrate	Base Pressure (×10 <sup>-3</sup> Pa)	Ar Pressure (Pa)	Bias Voltage (V)	Temperature (°C)	MoS <sub>2</sub> Current (A)	Deposition Time (min)	Zr Current (A)
Cemented carbide	6.5 ± 0.1	0.5 ± 0.2	−200	180 ± 10	1.6 ± 0.1	100 ± 5	0–100

The adhesive force and thickness of the coatings were measured with a material surface properties tester (MT-4000, Lanzhou Institute of Chemical Physics, Lanzhou, China), by scratching a diamond stylus of radius 200  $\mu\text{m}$  on the sample surface. The test conditions of adhesive force: applied load 100 N, scratch distance 10 mm, scratch speed 100 N/min; the test conditions of coating thickness: sliding distance 6 mm, test time 60 s. The coating surface hardness was measured on a microhardness tester (MH-6, Shanghai Testing Instrument Co., Ltd., Shanghai, China) at an applied load of 0.1 N. The surface topography of the composite coatings was detected by optical profiling system (Wyko NT9300, Veeco Inc., Plainview, NY, USA).

## 2.2. Wear Tests

The friction and wear tests were carried out on a block-on-ring tribometer (MRH-3, Shijin, Jinan, China). The schematic diagram of the tribometer is indicated in Figure 1. The block above ( $16 \times 16 \times 4.5$  mm) was a carbide specimen coated with the  $\text{MoS}_2\text{-Zr}$  lubricating coatings. The counterpart below was an AISI 5140 hardened steel ring with a dimension of  $50 \times 35 \times 15$  mm and surface hardness of HRC 46–50. Its main composition is about 97.5–97.7% Fe, 0.37–0.44% C, 0.80–1.10% Cr, 0.17–0.37% Si and 0.50–0.80% Mn. The upper specimen was mounted in a fixture without movement, and the lower ring was rotated with a speed of 260 mm/s and an applied load of 10 N. The average friction coefficient was the ratio of the tangential force to the normal force. The friction test conditions are shown in Table 3.

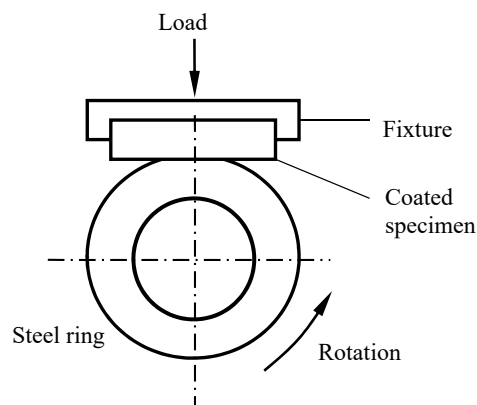


Figure 1. Schematic diagram of tribometer.

Table 3. The friction test conditions.

Speed (mm/s)	Load (N)	Ambient Temperature ( $^{\circ}\text{C}$ )	Humidity
260	10	20	40%–45%

All the experiments were repeated three times and the average values were presented. To determine the tribological characteristics of the  $\text{MoS}_2\text{-Zr}$  lubricating coatings, investigations were also performed through scanning electron microscope (SEM, INCA Penta FETXS, Oxford, UK) and energy dispersive X-ray spectrometer (EDX, D8 ADVANCE, Bruker, Germany).

## 3. Results and Discussion

### 3.1. Mechanical Properties

The surface morphologies of the composite coatings with different Zr content are shown in Figure 2. Figure 2a shows the SEM micrograph of pure  $\text{MoS}_2$  coating without the addition of Zr. Because the thickness of the pure  $\text{MoS}_2$  coating was just about 0.55  $\mu\text{m}$ , the grain structure of WC/TiC/Co substrate can still be seen through the surface coating. Figure 2b–f show the micrographs of the

MoS<sub>2</sub>-Zr composite coatings with the Zr current from 30 A to 100 A. The substrate surface with composite coatings can no longer be seen owing to a significant increase in thickness. However, the surface voids of the composite coatings were obvious, and the number void increased with Zr current, which can lead to an increase of surface roughness. Figure 3 shows the coating surface topography measured by the NT9300 optical profiling tester, and the average values of coating surface roughness under different Zr current are summarized in Figure 4. As shown in these figures, the coating surface became rougher with the increase of Zr current. The pure MoS<sub>2</sub> coating exhibited the minimum surface roughness ( $R_a 49 \pm 5$  nm), and the composite coatings with the Zr current of 100 A revealed the roughest topography with the roughness of  $R_a 91 \pm 5$  nm, which was consistent with the surface morphologies in Figure 2. This was probably because the increasing deposition current of Zr target resulted in the much stronger ion bombardment effect on the coating surface [36].

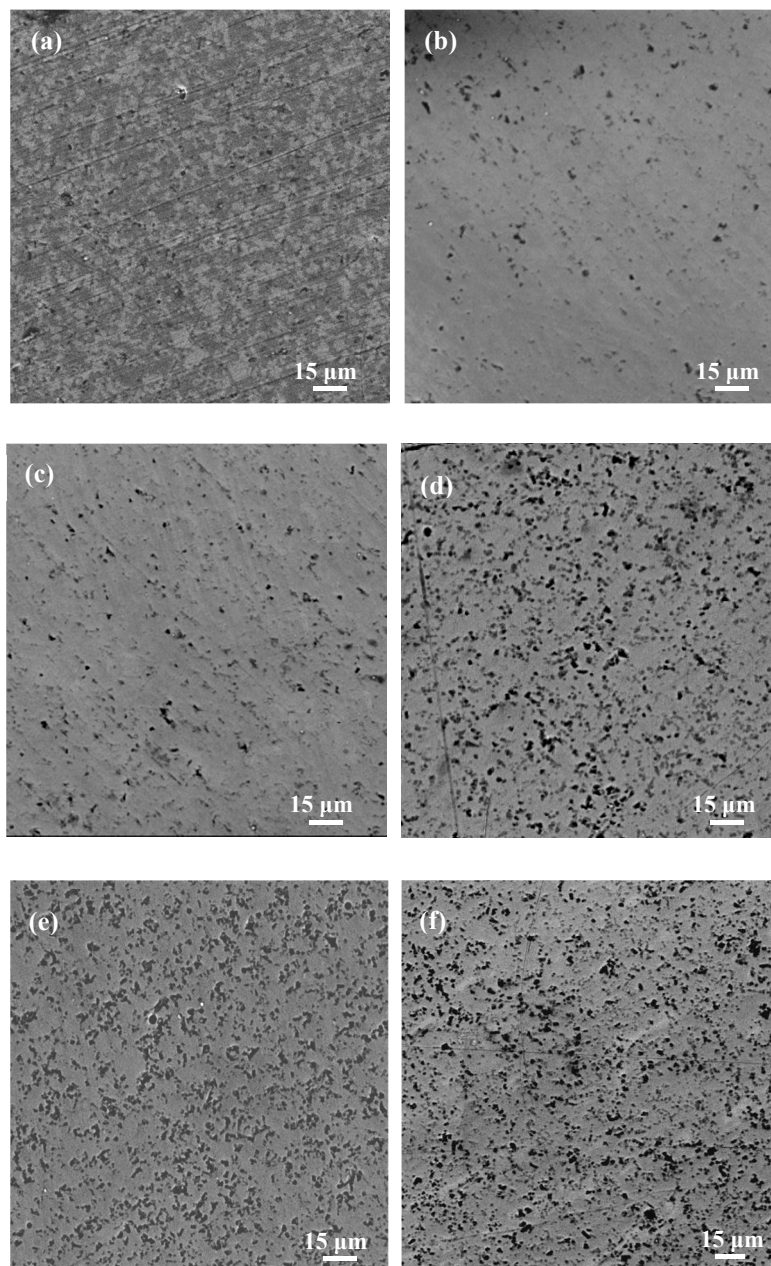


**Figure 2.** Surface morphologies of the composite coatings with different Zr current (a) 0 A; (b) 30 A; (c) 45 A; (d) 60 A; (e) 80 A; (f) 100 A.

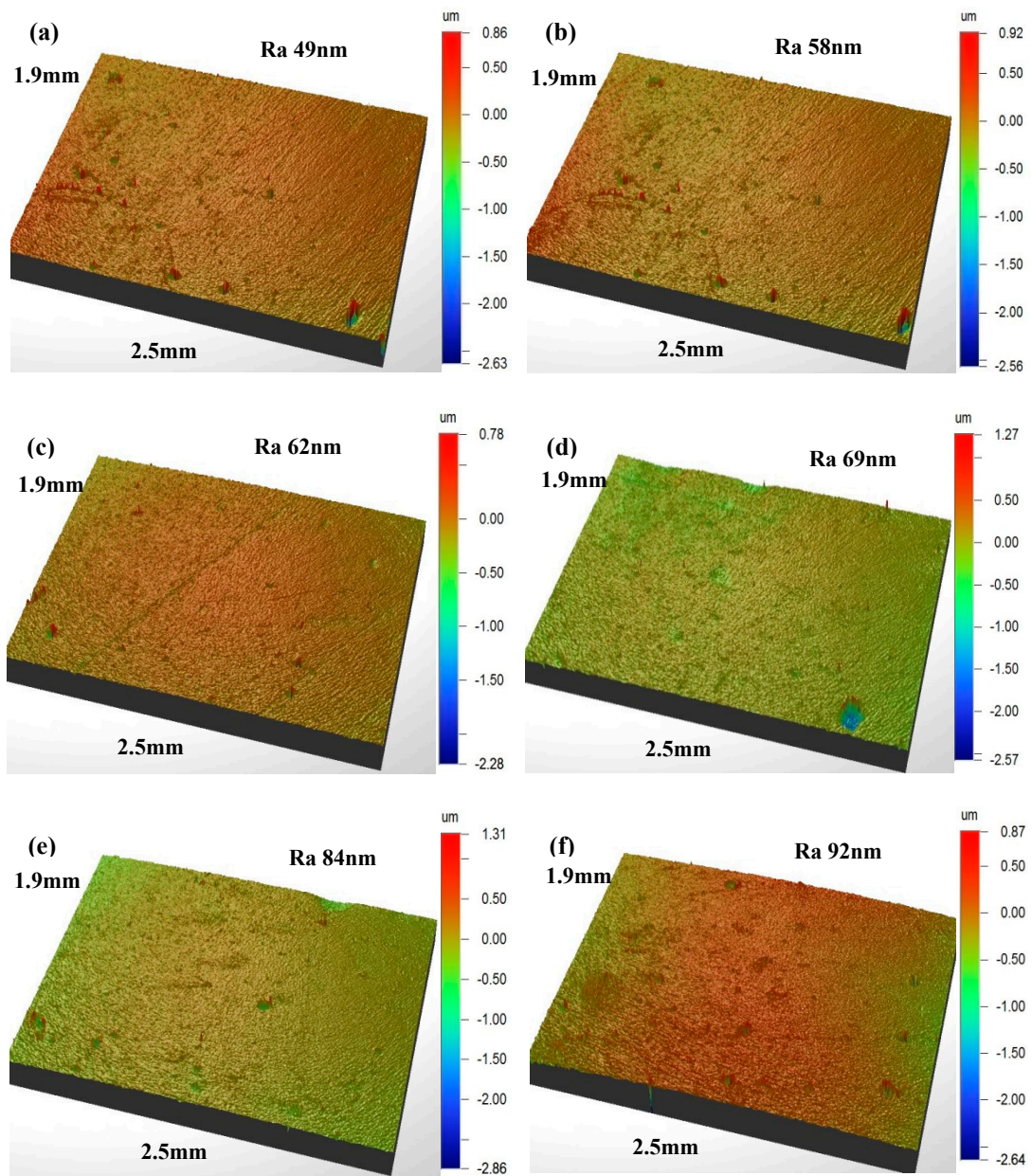


**Figure 3.** Surface topography of the composite coatings detected by a white light interferometer at different Zr current (a) 0 A; (b) 30 A; (c) 45 A; (d) 60 A; (e) 80 A; (f) 100 A.

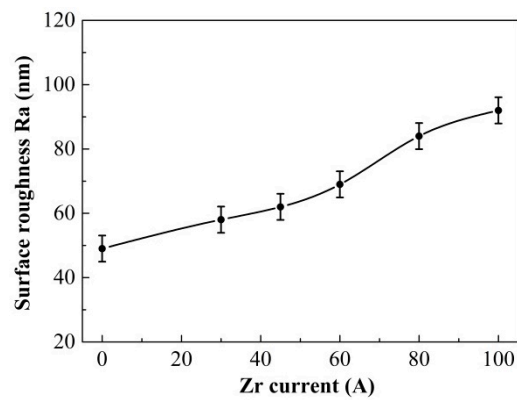


**Figure 4.** Surface roughness of the composite coatings.

Figure 5 shows the X-ray diffraction analysis result of the MoS<sub>2</sub>-Zr coatings with the Zr current of 30 A. It revealed that a very broadband pattern indicating a structure consisting of quasi-amorphous MoS<sub>2</sub>, and so it would appear that the addition of Zr into MoS<sub>2</sub> coating led to the vanishing of MoS<sub>2</sub> crystalline phase. It was also reported by the previous findings that the addition of metal (Ti, Cr, Zr, etc.) to MoS<sub>2</sub> to form the MoS<sub>2</sub>/metal composite coatings has resulted in the distortion of MoS<sub>2</sub> lattice parameters and X-ray amorphous microstructure [24,28,29,32].

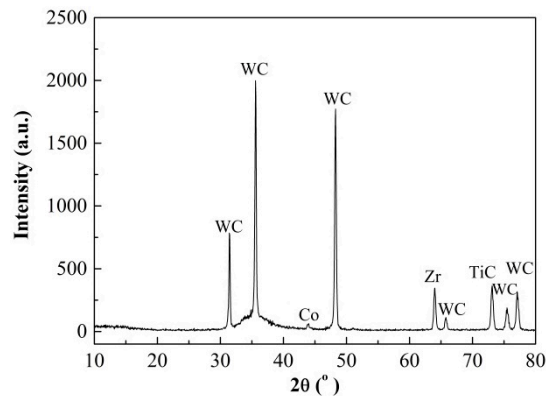


Figure 5. X-ray diffraction analysis of the composite coatings with Zr current of 30 A.

Figure 6 illustrates the weight content of Zr element in the composite coatings with different depositing current of Zr target. It was evident that the Zr content in coatings was in direct proportion with the current, owing to the improved deposition power and rate. As the current increased from 30 A to 100 A, the weight content of Zr element in composite coatings was increased from about 15% to 90%.

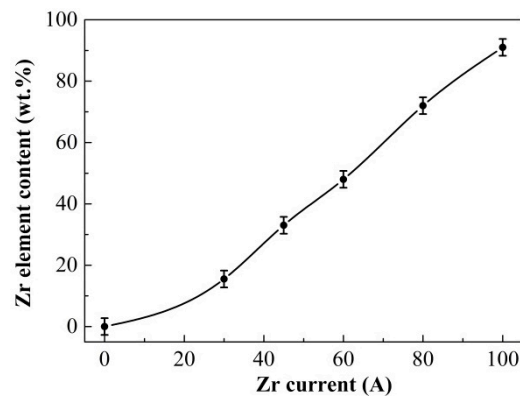


Figure 6. Weight content of the Zr element in the composite coatings.

The adhesive force between the substrate and coating was determined by the curve slope of friction coefficient and friction force owing to the coating spalling. The curves of the friction coefficient and friction force in the scratch test are plotted in Figure 7. From the figure, the curves were relatively steady and smooth at the beginning of the scratch test. As the scratch load increased to 58 N, the coatings scraped off gradually, and the curves of friction coefficient and friction force began to increase rapidly; when the load exceeded 64 N, the test curves both reached steady state with relatively high values owing to the wear and tear off of coatings. The adhesive force of the coatings at Zr current of 30 A was determined as about 58 N. Figure 8 shows the average value of adhesive force at different deposition current of Zr. It revealed that the adhesive force increased and reached the maximum value (68 N) at 45 A with the increase of Zr current. However, a further increase of deposition current may lead to the decrease of adhesive force, from about 63 N at 60 A down to 53 N at 100 A.

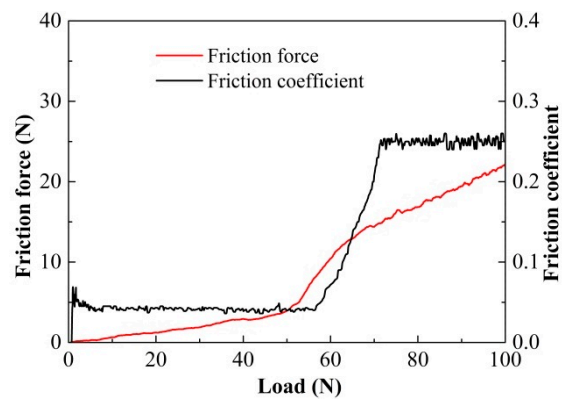


Figure 7. Adhesive force curve in scratch test with the Zr current of 30 A.

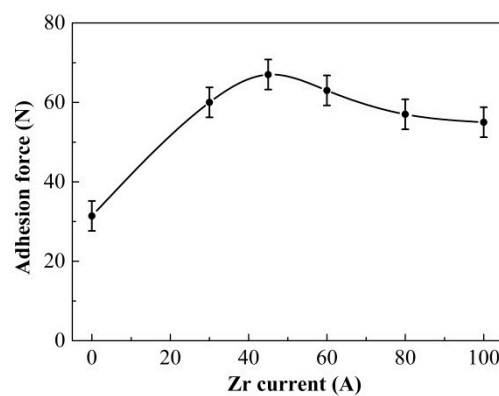


Figure 8. Adhesive force between the coatings and substrate.

The coating thickness was obtained by testing the height difference between the uncoated substrate and coating. The surface topography of the coating-substrate interface is shown in Figure 9. Figure 10 illustrates the curve of coating thickness in the scratch test at Zr current of 30 A, and Figure 11 exhibits the average value of coating thickness with various Zr current. It can be found that the coating thickness ran in a linear increase with the Zr current increase. As the current increased from 0 A to 100 A, the thickness was increased from 0.55  $\mu\text{m}$  to 2.91  $\mu\text{m}$ .

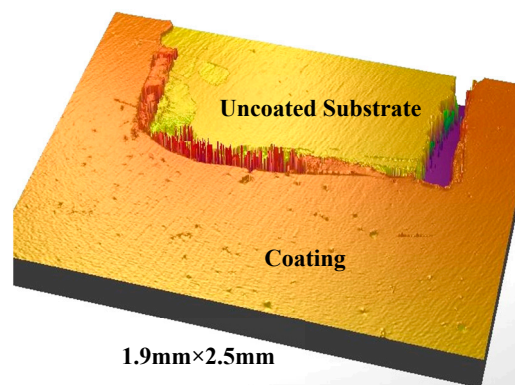


Figure 9. The surface topography of the coating-substrate interface.

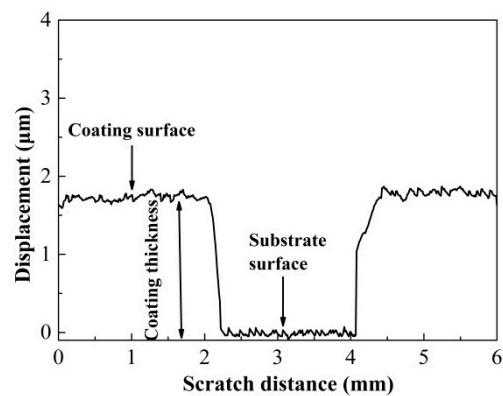


Figure 10. Coating thickness curve in scratch test with the Zr current of 30 A.

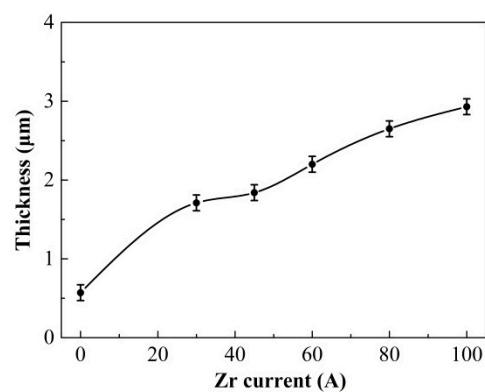


Figure 11. Coating thickness of the composite coatings.

Figure 12 shows the surface micro-hardness of the composite coatings. It was evident that the addition of Zr in the MoS<sub>2</sub>-Zr lubricating coatings was extremely helpful for the improvement of coating hardness, and more Zr content in the composite coatings led to higher hardness. The surface hardness of the pure MoS<sub>2</sub> coating was only 3.4 GPa, while the hardness of MoS<sub>2</sub>-Zr composite coatings was increased along with the increase of Zr current, from 7.8 GPa at 30 A up to 11.1 GPa at 100 A.

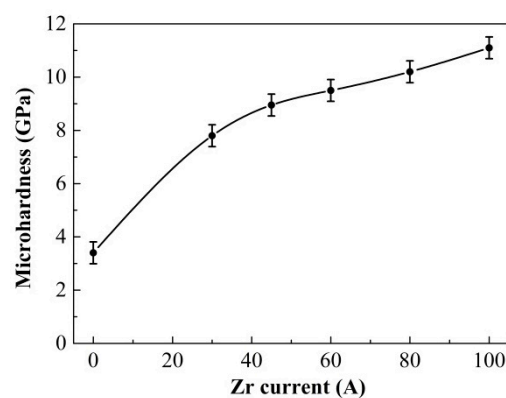


Figure 12. Micro-hardness of the composite coatings.

It is generally considered that the increasing current of target is beneficial to improve the deposition power, which is helpful to increase the coating compactness and deposition rate. The increased coating compactness is conducive to improving the adhesive force and surface hardness, while the improved deposition rate contributes to the increase of coating thickness, which has been confirmed by the test results as shown in Figures 8, 11 and 12. However, further increase of deposition current of target may

lead to the decrease of adhesive force, which might be attributed to the high intrinsic stress caused by excessive solid solution strengthening of Zr element [36].

In addition, the coating thickness can affect the adhesive force of the coating to the substrate. The intrinsic stress  $\sigma_b$  of the coating can be expressed by [36]:

$$\sigma_b = \frac{1.22E_c}{1 - \nu_c^2} \left(\frac{t}{r}\right)^2 \quad (1)$$

where  $\nu_c$  and  $E_c$  are the Poisson ratio and Young's Modulus of the coating, respectively,  $t$  is the coating thickness and  $r$  is the radius of the circular region of interfacial detachment.

When the coating thickness increases from 0.55  $\mu\text{m}$  to 2.91  $\mu\text{m}$  (see Figure 11), the intrinsic stress  $\sigma_b$  will be increased by nearly 25 times according to Equation (1). Then the adhesive force between the coating and substrate could be decreased, and this is in accordance with the result of adhesive force as shown in Figure 8.

### 3.2. Tribological Behaviors of Composite Coatings

The current of Zr target clearly affected the surface morphologies, surface roughness, Zr content, adhesive force, thickness, and microhardness, which would change the friction behaviors and wear modes of the coatings. Figure 13 illustrates the average friction coefficients of the composite coatings at the speed of 260 mm/s and a normal load of 10 N. At the beginning of the friction test (Figure 13), the friction coefficients of the composite coatings increased with the increasing Zr current. The pure MoS<sub>2</sub> coating possessed the optimum lubrication performance with the friction coefficient of about 0.03, while the composite coatings with the Zr current of 100 A presented the highest friction coefficient of about 0.3, which was obviously higher than the other composite coatings with lower current.

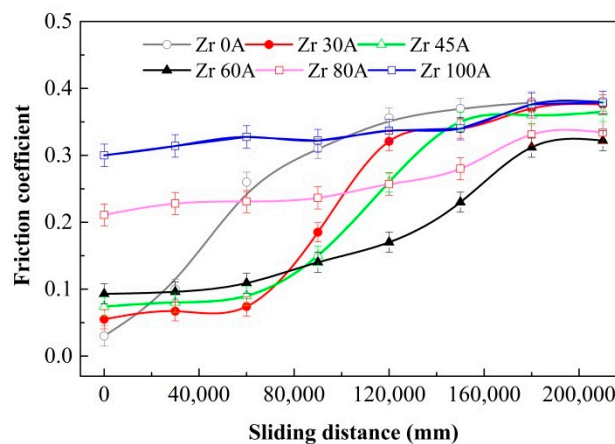


**Figure 13.** Effect of Zr current on the average friction coefficient of coatings (sliding speed 260 mm/s, applied load 10 N).

As the friction test went on, the curves of the friction coefficient exhibited different variations trend. The friction coefficient of the coatings gradually increased, and the lower of the Zr current, the faster the friction curve rose. This could be attributed to the effects of deposition current on the mechanical properties of the coatings, such as the adhesive force, surface hardness, thickness and their integrated effects. Compared to those of the coated samples at deposition current of lower than 60 A, the friction coefficients of coatings at higher current kept stable at relatively high values.

### 3.3. Wear Properties and Discussion

To determine the friction and wear characteristics of the test samples, SEM and EDX were applied to investigate the morphologies and element composition of the worn surface. The worn micrograph

and corresponding EDX composition analysis are illustrated in Figures 14 and 15. As shown in Figure 14a, the pure MoS<sub>2</sub> coating was almost worn out. There existed obvious scratched appearance on the wear track. The corresponding surface composition analyses of points A and B in Figure 14a are indicated in Figure 15a,b. The Mo and S elements of the coatings were not tested in the worn area (Figure 15b), and the Fe and O elements except the elements of carbide substrate were also confirmed on the worn track. It could be considered that the main wear forms of the sample coated with the pure MoS<sub>2</sub> coatings were abrasive and adhesive wear. The wear characteristic was consistent with the curve variation of the friction coefficient for the MoS<sub>2</sub> coating shown in Figure 13. Pure MoS<sub>2</sub> coating exhibited the best lubrication performance at the beginning of the test, while the coating failed easily and friction coefficient increased soon due to the lower coating hardness and adhesive force.

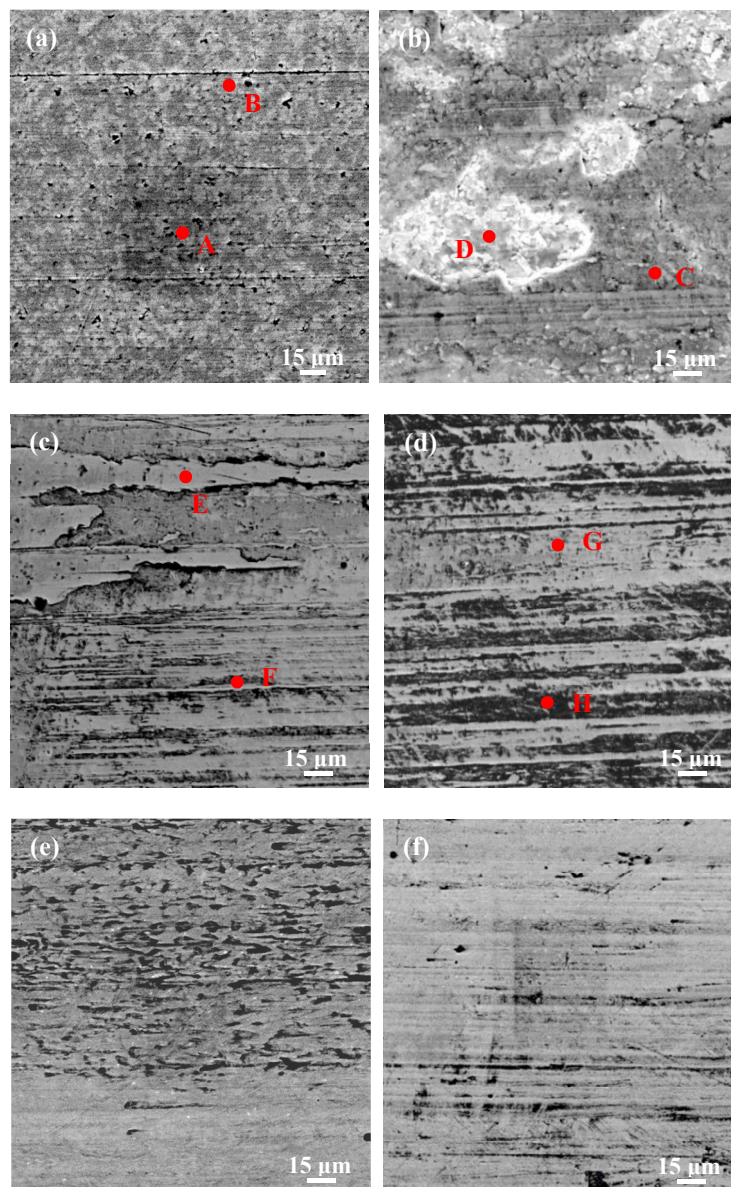


**Figure 14.** The morphologies of the worn surface of the composite coatings (a) 0 Al; (b) 30 Al; (c) 45 Al; (d) 60 Al; (e) 80 Al; (f) 100 Al (conditions: load 10 N, sliding speed 260 mm/s, sliding distance 90,000 mm).

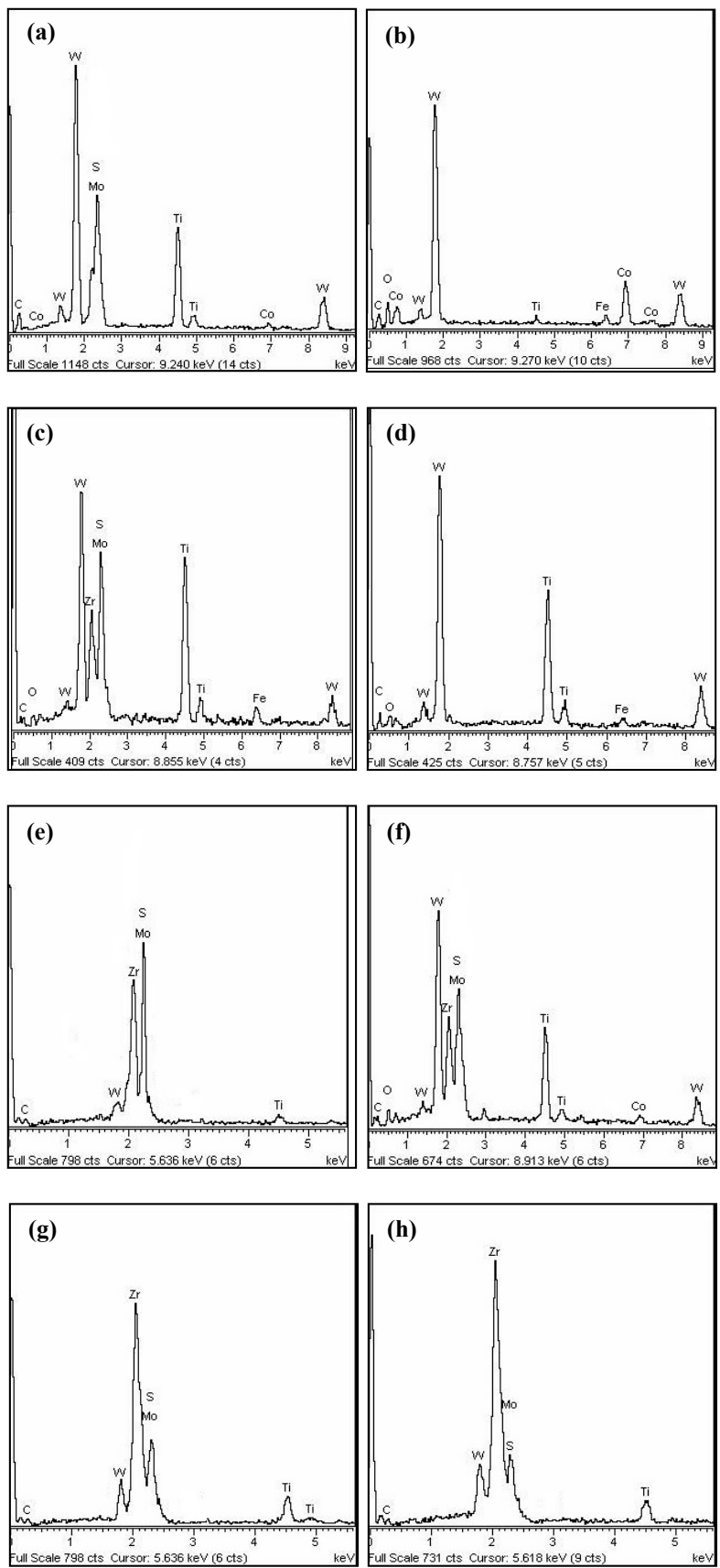


**Figure 15.** The corresponding EDX composition analysis of points A–H in Figure 14: (a) point A; (b) point B; (c) point C; (d) point D; (e) point E; (f) point F; (g) point G; (h) point H.

The worn micrograph and corresponding EDX composition analysis of the composite coatings deposited at the Zr current of 30 A are shown in Figure 14b, Figure 15c,d. From these figures, serious flaking of the coatings and abrasive wear could be observed in the worn area. Compared with the pure MoS<sub>2</sub> coating, the composite coatings with the addition of Zr could improve the wear resistance and prolong the service time, due to the higher hardness and adhesive force. At the same time, it could be found that there also existed a bit of adhesive wear due to the existence of Fe and O element in Figure 15c,d.

Figure 14c illustrates the worn micrograph of the coatings prepared at the Zr current of 45 A. It revealed that there were some coating delamination and plowing grooves on the wear track. Figure 15e,f indicated the corresponding element analysis of point E and F in Figure 14c. It demonstrated that the adhesive materials were mainly composed of the MoS<sub>2</sub>-Zr coatings and the oxides. Delamination and abrasive wear were the main wear forms.

From Figures 14d-f and 15g-h, it indicated that the main wear mode of the composite coatings at deposition current of higher than 60 A was mainly abrasive wear. It was also found that the abrasive wear of the composite coatings was slightly reduced with the increase of current from 60 A to 100 A.

As shown in the test results above, it was considered that the friction behaviors and wear characteristics of the friction pairs depended on the components and mechanical properties of the composite coatings caused by various Zr current. The lower Zr current was conducive to increasing the content of MoS<sub>2</sub> in the composite coatings, promoting the lubricating performances and lowering the friction coefficient; while the higher Zr current was beneficial to increase the content of Zr element in the coatings, improve the wear resistance and extend the service life, due to the more excellent adhesive force, higher surface hardness, thickness, and their integrated effects.

The future investigation work will be carried out on the morphology, microstructure, tribological properties of MoS<sub>2</sub>-Zr coatings under different test conditions (humidity, temperature, etc.), and the dynamic crack resistance.

#### 4. Conclusions

The MoS<sub>2</sub>-Zr lubricating coatings were prepared on the WC/TiC/Co carbide surface utilizing duplex depositing technology. The effects of different Zr target current on the performance of the composite coatings were studied. The primary conclusions were obtained as below:

- (1) The properties of the MoS<sub>2</sub>-Zr coatings prepared by adding Zr additives can be significantly improved compared to those of the pure MoS<sub>2</sub> coating.
- (2) As the deposition current of Zr target increased, the surface roughness, Zr content, thickness and micro-hardness of coatings gradually increased, while the adhesive force first increased and then decreased.
- (3) The tribological behaviors and wear forms of the coatings both varied obviously with the increase of Zr current. At the beginning of the friction test, the average friction coefficient of the composite coatings was increased with the increasing Zr, while the wear resistance and service life were improved.
- (4) The mechanism responsible for the differences of tribological performance was mainly attributed to the different mechanical properties of the coatings caused by various Zr current.

**Author Contributions:** W.S. conceived and designed the experiments; Z.X. and S.W. performed the experiments; Q.Z. analyzed the data; W.S. wrote the paper. All authors have read and agreed to the published version of the manuscript.

**Funding:** This research was funded by the Key Research and Development Program of Shandong Province (Grant No. 2017GGX203007) and Postdoctoral Innovative Projects of Shandong Province (Grant No. 201603028).

**Acknowledgments:** This work was supported by the Talent Project of Jining University.

**Conflicts of Interest:** The authors declare no conflict of interest.

## References

1. Holmberg, K.; Matthews, A. *Coatings Tribology: Properties, Mechanisms Techniques and Applications in Surface Engineering*; Elsevier Science: Amsterdam, The Netherland, 2009; pp. 1–14.
2. Bashir, M.I.; Shafiq, M.; Naeem, M.; Zaka-Ul-Islam, M.; Díaz-Guillén, J.C.; LopezBadillo, C.M.; Zakaullah, M. Enhanced surface properties of aluminum by PVD-TiN coating combined with cathodic cage plasma nitriding. *Surf. Coat. Technol.* **2017**, *327*, 59–65. [[CrossRef](#)]
3. Dhandapani, V.S.; Subbiah, R.; Thangavel, E.; Arumugam, M.; Park, K.; Gasem, Z.M.; Veeraragavan, V.; Kim, D.E. Tribological properties, corrosion resistance and biocompatibility of magnetron sputtered titanium-amorphous carbon coatings. *Appl. Surf. Sci.* **2016**, *371*, 262–274. [[CrossRef](#)]
4. Goel, S.; Björklund, S.; Curry, N.; Wiklund, U.; Joshi, S.V. Axial suspension plasma spraying of Al<sub>2</sub>O<sub>3</sub> coatings for superior tribological properties. *Surf. Coat. Technol.* **2017**, *315*, 80–87. [[CrossRef](#)]
5. Vereschaka, A.A.; Bublikov, J.I.; Sitnikov, N.N.; Oganyan, G.V.; Sotova, C.S. Influence of nanolayer thickness on the performance properties of multilayer composite nano-structured modified coatings for metal-cutting tools. *Int. J. Adv. Manuf. Technol.* **2018**, *95*, 2625–2640. [[CrossRef](#)]
6. Antonov, M.; Afshari, H.; Baronins, J.; Adoberg, E.; Raadik, T.; Hussainova, I. The effect of temperature and sliding speed on friction and wear of Si<sub>3</sub>N<sub>4</sub>, Al<sub>2</sub>O<sub>3</sub>, and ZrO<sub>2</sub> balls tested against AlCrN PVD coating. *Tribol. Int.* **2018**, *118*, 500–514. [[CrossRef](#)]
7. Rosa, G.C.; Souza, A.J.; Possamai, E.V.; Amorim, H.J.; Neis, P.D. Wear analysis of ultra-fine grain coated carbide tools in hard turning of AISI 420C stainless steel. *Wear* **2017**, *376–377*, 172–177. [[CrossRef](#)]
8. Arulkirubakaran, D.; Senthilkumar, V. Performance of TiN and TiAlN coated micro-grooved tools during machining of Ti-6Al-4V alloy. *J. Refract. Met. Hard Mater.* **2017**, *62*, 47–57. [[CrossRef](#)]
9. Wu, Z.; Zhou, F.; Wang, Q.; Zhou, Z.; Yan, J.; Li, K. Influence of trimethylsilane flow on the microstructure, mechanical and tribological properties of CrSiCN coatings in water lubrication. *Appl. Surf. Sci.* **2015**, *355*, 516–530. [[CrossRef](#)]
10. Ma, Q.; Li, L.; Xu, Y.; Ma, X.; Xu, Y.; Liu, H. Effect of Ti content on the microstructure and mechanical properties of TiAlSiN nanocomposite coatings. *J. Refract. Met. Hard Mater.* **2016**, *59*, 114–120. [[CrossRef](#)]
11. He, N.; Li, H.; Ji, L.; Liu, X.H.; Zhou, H.D.; Chen, J.M. High temperature tribological properties of TiAlSiN coatings produced by hybrid PVD technology. *Tribol. Int.* **2016**, *98*, 133–143. [[CrossRef](#)]
12. Tillmann, W.; Dildrop, M. Influence of Si content on mechanical and tribological properties of TiAlSiN PVD coatings at elevated temperatures. *Surf. Coat. Technol.* **2017**, *321*, 448–454. [[CrossRef](#)]
13. Bushlya, V.; Johansson, D.; Lenrick, F.; Ståhl, J.E.; Schultheiss, F. Wear mechanisms of uncoated and coated cemented carbide tools in machining lead-free silicon brass. *Wear* **2017**, *376–377*, 143–151. [[CrossRef](#)]
14. Lian, Y.S.; Deng, J.X.; Li, S.P.; Xing, Y.Q.; Chen, Y.Y. Preparation and cutting performance of WS<sub>2</sub>, soft-coated tools. *Int. J. Adv. Manuf. Technol.* **2013**, *67*, 1027–1033. [[CrossRef](#)]
15. Deng, J.X.; Lian, Y.S.; Wu, Z.; Xing, Y.Q. Performance of femtosecond laser-textured cutting tools deposited with WS<sub>2</sub>, solid lubricant coatings. *Surf. Coat. Technol.* **2013**, *222*, 135–143. [[CrossRef](#)]
16. Li, S.P.; Deng, J.X.; Yan, G.Y.; Zhang, K.D.; Zhang, G.D. Microstructure, mechanical properties and tribological performance of TiSiN-WS<sub>2</sub> hard-lubricant coatings. *Appl. Surf. Sci.* **2014**, *309*, 209–217. [[CrossRef](#)]
17. Meng, R.; Deng, J.X.; Liu, Y.Y.; Duan, R.; Zhang, G. Improving tribological performance of cemented carbides by combining laser surface texturing and W-S-C solid lubricant coating. *Int. J. Refract. Met. Hard Mater.* **2018**, *72*, 163–171. [[CrossRef](#)]
18. Fan, H.Z.; Hu, T.C.; Wan, H.Q.; Zhang, Y.S.; Song, J.J.; Hu, L.T. Surface composition-lubrication design of Al<sub>2</sub>O<sub>3</sub>/Ni laminated composites-Part II: Tribological behavior of LaF<sub>3</sub>-doped MoS<sub>2</sub> composite coating in a water environment. *Tribol. Int.* **2016**, *96*, 258–268. [[CrossRef](#)]
19. Luo, J.; Zhu, M.H.; Wang, Y.D.; Zheng, J.F.; Mo, J.L. Study on rotational fretting wear of bonded MoS<sub>2</sub> solid lubricant coating prepared on medium carbon steel. *Tribol. Int.* **2011**, *44*, 1565–1570. [[CrossRef](#)]
20. Shi, M.S. *Solid Lubricating Materials*; China Chemical Industry Press: Beijing, China, 2000; pp. 127–146.
21. Fouvry, S.; Paulin, C. An effective friction energy density approach to predict solid lubricant friction endurance: Application to fretting wear. *Wear* **2014**, *319*, 211–226. [[CrossRef](#)]
22. Martins, R.C.; Paulo, S.M.; Seabra, J.O. MoS<sub>2</sub>/Ti low-friction coating for gears. *Tribol. Int.* **2006**, *39*, 1686–1697. [[CrossRef](#)]

23. Bhaduri, D.; Kumar, R.; Jain, A.K.; Chattopadhyay, A.K. On tribological behaviour and application of tin and MoS<sub>2</sub>-Ti composite coating for enhancing performance of monolayer CBN grinding wheel. *Wear* **2010**, *268*, 1053–1065. [[CrossRef](#)]
24. Renevier, N.M.; Lobiondo, N.; Fox, V.C.; Teer, D.G.; Hampshire, J. Performance of MoS<sub>2</sub>/metal composite coatings used for dry machining and other industrial applications. *Surf. Coat. Technol.* **2000**, *123*, 84–91. [[CrossRef](#)]
25. Renevier, N.M.; Fox, V.C.; Teer, D.G.; Hampshire, J. Performance of low friction MoS<sub>2</sub> titanium composite coatings used in forming applications. *Mater. Des.* **2000**, *21*, 337–343. [[CrossRef](#)]
26. Su, Y.L.; Kao, W.H. Tribological behaviour and wear mechanism of MoS<sub>2</sub>-Cr coatings sliding against various counterbody. *Tribol. Int.* **2003**, *36*, 11–23. [[CrossRef](#)]
27. Kao, W.H. Tribological properties and high speed drilling application of MoS<sub>2</sub>-Cr coatings. *Wear* **2005**, *258*, 812–825. [[CrossRef](#)]
28. Renevier, N.M.; Fox, V.C.; Teer, D.G.; Hampshire, J. Coating characteristics and tribological properties of sputter-deposited MoS<sub>2</sub>/metal composite coatings deposited by closed field unbalanced magnetron sputter ion plating. *Surf. Coat. Technol.* **2000**, *127*, 24–37. [[CrossRef](#)]
29. Man, Y.; Zhang, G.J.; Ba, Y.W.; Wang, T.; Wang, X.; Liu, Z.N. Microstructure and tribological properties of MoS<sub>2</sub>+Zr composite coatings in high humidity environment. *Appl. Surf. Sci.* **2016**, *367*, 140–146. [[CrossRef](#)]
30. Deng, J.X.; Song, W.L.; Zhang, H.; Zhao, J.L. Friction and wear behaviours of MoS<sub>2</sub>/Zr coatings against hardened steel. *Surf. Eng.* **2008**, *24*, 410–415. [[CrossRef](#)]
31. Song, W.L.; Wang, Z.C.; Deng, J.X.; Zhou, K.; Wang, S.J.; Guo, Z.X. Cutting temperature analysis and experiment of Ti-MoS<sub>2</sub>/Zr-coated cemented carbide tool. *Int. J. Adv. Manuf. Technol.* **2017**, *93*, 799–809. [[CrossRef](#)]
32. Deng, J.X.; Song, W.L.; Zhang, H.; Zhao, J.L. Performance of PVD MoS<sub>2</sub>/Zr-coated carbide in cutting processes. *Int. J. Mach. Tool Manuf.* **2008**, *48*, 1546–1552. [[CrossRef](#)]
33. Song, W.L.; Deng, J.X.; Yan, P.; Wu, Z.; Zhang, H.; Zhao, J.; Ai, X. Influence of Negative Bias Voltage on the Mechanical and Tribological Properties of MoS<sub>2</sub>/Zr Composite Films. *J. Wuhan Univ. Technol.* **2011**, *26*, 412–416. [[CrossRef](#)]
34. Güler, E.S.; Karakaya, İ.; Konca, E. Effects of current density, coating thickness, temperature, pH and particle concentration on internal stress during Ni-MoS<sub>2</sub> electrocodeposition. *Surf. Eng.* **2014**, *30*, 109–114. [[CrossRef](#)]
35. Li, H.; Zhang, G.; Wang, L. Low humidity-sensitivity of MoS<sub>2</sub>/Pb nanocomposite coatings. *Wear* **2015**, *350*, 1–9. [[CrossRef](#)]
36. Xiong, D.S.; Li, J.L. *Solid Lubrication Coating Technology for Special Environments*; National Defense Industry Press: Beijing, China, 2016; pp. 2–78.

